Bioresource Technology 405 (2024) 130934

Contents lists available at ScienceDirect

Bioresource Technology

journal homepage: www.elsevier.com/locate/biortech

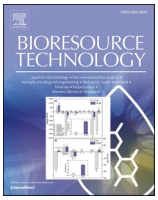

Fast screening of catalyst performances in hydrothermal processes for biofuel production using differential scanning calorimetry

Vittoria Benedetti [a,*], Alessandro Cascioli [a], Matteo Pecchi [b], Marco Baratieri [a]

[a] Faculty of Engineering, Free University of Bozen-Bolzano, Piazza Domenicani 3, Bozen-Bolzano 39100 Italy
[b] Department of Biological and Environmental Engineering, Cornell University, 111 Wing Drive, Ithaca 14853, NY, United States

HIGHLIGHTS

- HP-DSC to evaluate catalyst behavior and performance under hydrothermal conditions.
- Mixtures of cellulose and heterogeneous catalysts tested at 250 °C.
- Siralox and $FeCl_3$ showed the highest catalytic activities.
- Investigation of synergies among acid and basic sites.

GRAPHICAL ABSTRACT

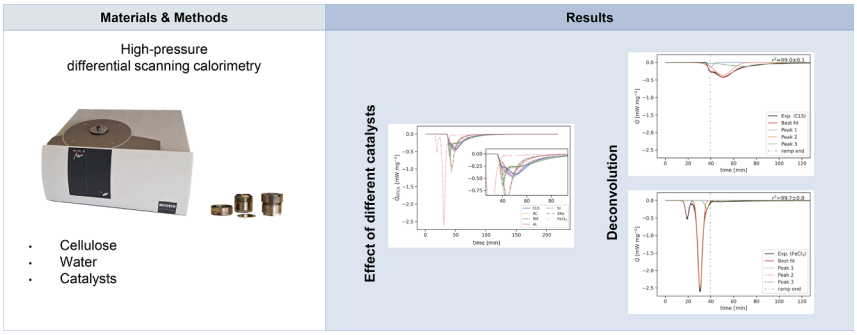

ARTICLE INFO

Keywords:
Hydrothermal carbonization
Cellulose
Heat release
DSC

ABSTRACT

Catalysts are usually employed in hydrothermal processes for different purposes, such as enhancing quality and yield of produced biofuels. However, assessing catalyst performances can be time consuming and expensive. For this reason, in this work, a technique based on high pressure differential scanning calorimetry was applied to study heterogeneous catalyst behavior under hydrothermal conditions at the micro-scale. Heterogeneous catalysts were mixed with distilled water and cellulose, selected as substrate, and tested at 250 °C. The heat release profiles obtained were deconvoluted in three Gaussian peaks, each associated with a set of reactions. Siralox and iron chloride showed the highest catalytic activities impacting the development and the enthalpy of the reactions. Selected samples were further characterized to investigate synergies among acid and basic sites and emphasize the importance of the spatial distribution of the components inside the catalysts. This study highlights the crucial role of advanced techniques in optimizing catalyst performance for more efficient biofuel production.

1. Introduction

The need for sustainable alternatives to fossil fuels is becoming increasingly urgent (World Energy Transitions Outlook 2022, 2022). The long-haul, aviation and marine transport sectors are the hardest to electrify, and hydrogen does not appear to be a viable solution considering the current state of the technology (Yue et al., 2021; Zhang et al., 2021). Hence, liquid fuels are still essential for these sectors, at least in

* Corresponding author.
E-mail address: vittoria.benedetti@unibz.it (V. Benedetti).

https://doi.org/10.1016/j.biortech.2024.130934
Received 8 April 2024; Received in revised form 22 May 2024; Accepted 6 June 2024
Available online 6 June 2024

the near future. In this scenario, hydrothermal processes – hydrothermal carbonization (HTC) and hydrothermal liquefaction (HTL) – can play a pivotal role exploiting hot pressurized water to produce fuels from wet waste streams usually disposed of in landfills (European Environment Agency, 2020; Timko et al., 2015). HTC takes place at temperatures between 180 and 250 °C under autogenous pressure (Libra et al., 2011). The main product is a coal-like solid material called hydrochar, which can be exploited as fuel or, after upgrading, as soil improver (Libra et al., 2011; Mahmood Al-Nuaimy et al., 2023). HTL involves more severe conditions, which can be near-supercritical or even supercritical, with temperature in the range 300–350 °C and pressure in the range 50–250 bar (Kumar et al., 2018). In this case, the main product is the biocrude, which can be further upgraded into drop-in biofuels following hydrogenation and distillation (Castello et al., 2018). To maximize product yields, shorten the reaction time, reduce energy consumption, and tune product properties according to final applications, catalysts can be added to the processes (Akbari et al., 2023; Sharma et al., 2021). In HTC, organic acids, alcohols, strong mineral acids and bases, metal chlorides, metal oxides, hydrogen peroxides, nitrate salts, sulfates, persulfates, and sulfites salts have been reported to impact hydrolysis, dehydration, carbonization reactions and glycoside bonds cleavage, affecting hydrochar porosity and the presence of oxygen functional groups on its surface (Chen et al., 2022; Djandja et al., 2023; Faradilla et al., 2020; Zhang et al., 2022). In HTL, catalysts are used to improve biocrude yield and quality, and inhibit char formation. Both homogeneous and heterogenous catalysts are currently under investigation, the former being more difficult to recover and requiring neutralization, the latter being easier to separate and usually less expensive (Cheng et al., 2020; Liu et al., 2018; Ross et al., 2010). Considering the target scale of HTC and HTL industrial plants, identifying inexpensive catalyst is necessary to demonstrate their economic feasibility. Cheng et al. studied the effect of adding red mud (also known as bauxite residues, an industrial waste from the aluminum production rich in different metal oxides) and red clay (cheap and abundant waste from the brick and tile industry) when processing food waste through HTL (Cheng et al., 2020); they obtained a 139 and 100 % increase in biocrude carbon yield and a 11 and 4 % increase in biocrude higher heating value (HHV) for red mud and red clay, respectively (Cheng et al., 2020). Moreover, according to this study, mixed oxides, such as red mud and red clay, showed better performances compared to single metal oxides due to the synergistic effects of the base and acid sites present on their surfaces (Cheng et al., 2020). Indeed, acid sites promote hydrolysis, dehydration, decarboxylation, and depolymerization accelerating the conversion, while base sites catalyze aldol condensation, amide formation, esterification and ketonization reactions governing the product distribution (Kellicutt et al., 2014; Sharma et al., 2007; Weingarten et al., 2011). Unfortunately, the traditional approach for assessing catalysts in HTC and HTL by means of batch tests and chemical analysis of products is time consuming and expensive, considering that each catalyst must be evaluated at each condition, both in terms of residence time and process temperature. An alternative approach that can significantly reduce time and costs, while providing a continuous in-situ and in-operando perspective on the process development, is high pressure differential scanning calorimetry (HP-DSC). In DSC, the heat flow produced or absorbed during the development of a thermally activated process (like HTC and HTL) is recorded continuously as the sample temperature changes. As far as pressurized systems are concerned, the challenge is to separate the heat released by the process from the sensible heat required to change the system temperature. In previous works, the authors proposed the baseline subtraction method to isolate and quantify the process signal, relying on DSC runs with the unreacted and reacted sample (Pecchi et al., 2020a). This method was demonstrated for the assessment of the enthalpy change of HTC and HTL (Pecchi et al., 2022, 2020a) and for the study of HTC kinetics (Pecchi et al., 2020b). Recently, other groups have adopted similar approaches (Ischia et al., 2022; Sudibyo et al., 2024). For instance, Hammerton et al. coupled DSC and HTC batch results to demonstrate that the addition of inorganic salts shifts the time onset of the exothermal peaks associated with HTC, suggesting that DSC can detect catalyst activity (Hammerton and Ross, 2022). In the present work, the exhaust baseline method is applied to quantify the effect of catalysts on the heat released by HTC (both in terms of magnitude and timing) using cellulose as substrate (Pecchi et al., 2022). In particular, the heat release profiles from HTC of cellulose with and without the presence of catalysts are assessed and further deconvoluted to discriminate the specific effect that each catalyst exerts on specific sets of bulk reactions (Pecchi et al., 2022).

2. Materials and methods

2.1. Feedstock

The feedstock used in this work is pure cellulose (99.5 %), purchased from Tebaldi Srl. Properties of cellulose (denoted as CLS in the manuscript) are reported in Table 1 (Pecchi et al., 2020a).

2.2. Catalysts

The catalysts tested include Silica fumed (CAS Number: 112945–52-5, Sigma-Aldrich denoted as SI), Aluminum oxide (CAS Number: 1344–28-1, Sigma-Aldrich, denoted as AL), Iron (III) chloride (CAS Number: 7705–08-0, Sigma-Aldrich, denoted as $FeCl_3$), Siralox40 (Sasol, denoted as SRa), Red clay (Argilez, denoted as RC), and Red mud (Eurallumina SpA, Italy, denoted as RM). For details regarding RC and RM characterization refer to the works of Cheng et al., and Sushil et al., respectively (Cheng et al., 2020; Sushil and Batra, 2008).

2.3. Differential scanning calorimetry experiments

DSC experiments methodology is described elsewhere (Pecchi et al., 2020a). Briefly, a Maia 200 F3 heat-flux DSC (NETZSCH GmbH) was used in combination with gold-plated Ni-steel high-pressure crucibles, with an internal volume of 100 µL and a nominal maximum pressure of 100 bar. In each test, 8 mg of cellulose and 46 mg of distilled water were added in the crucible, with 2.8 mg of catalyst and shaken vigorously. The filled crucible was placed in the DSC furnace along with an empty reference crucible. The temperature program, a combination of isothermal and non-isothermal steps, was run twice without moving the crucibles. The temperature program started with a stabilization step at 50 °C, which lasted 15 min. This step was followed by a heating step, with a heating rate of 5 °C min^{-1}, up to the set temperature (250 °C), which was then kept constant for 3 h. The initial step was crucial for the data processing as it represents a common starting point for the two runs. The crucible was weighed before and after the experiment. If any pre/post run mass difference above 2 % was noted, the run was discarded and repeated. Each test was repeated at least twice to ensure repeatability. The data collected were analyzed and deconvoluted with the same methodology described in previous work (Pecchi et al., 2022). In short, the peak deconvolution of the heat release profile was performed using the "Gaussian Model" class from the "lmfit" Python package (Newville et al., 2014). The fit involved three exothermal peaks,

Table 1
Cellulose properties [19].

	Unit	Cellulose
Moisture	%wt	6.14 ± 0.02
Ash	$\%wt_{dry}$	0.21 ± 0.09
C	$\%wt_{dry}$	44.04 ± 0.25
H	$\%wt_{dry}$	6.00 ± 0.10
N	$\%wt_{dry}$	0.06 ± 0.02
S	$\%wt_{dry}$	0.14 ± 0.03
O	$\%wt_{dry}$	49.54 ± 0.31
HHV	MJ/kg	16.21 ± 0.05

with the first peak having a maximum center location at 40 min and maximum characteristic width of 25 as constraints. The first-guess center values were 38, 50, and 80 min for the three peaks. The only exception occurred in the case of $FeCl_3$, which dramatically anticipates the start of the reaction and therefore required first-guess of 15, 26, and 60 min for the three peaks. The deconvolution was performed on each experiment individually and the results averaged.

2.4. Characterization of catalysts

Sample phases were investigated by X-ray diffraction (XRD) technique. X-ray powder diffraction patterns were collected at room temperature, with a scan rate of 1°/80 sec at 40 kV and 40 mA, using a PANalytical Empyrean diffractometer (Bragg-Brentano parafocusing geometry) equipped with a PIXcel3D-Medipix3 1x1 area detector and Cu – Kα radiation (λ = 1.5418 Å). Moreover, a FT-IR, Tensor 27 (Bruker), equipped with Platinum ATR was used to analyze the catalysts. A resolution of 4 cm^{-1} and 16 scans was chosen as trade-off among scanning time, absence of artifacts, and fair signal to noise ratio. The analysis was performed in triplicate.

3. Results and discussion

3.1. Results using the exhaust baseline subtraction method and peak deconvolution

Results of the DSC runs with cellulose with and without the addition of catalysts are plotted in Fig. 1. The baseline subtraction method has been extensively explained and validated in previous works (Pecchi et al., 2022, 2020a). In the present study, only corrected values are considered. Fig. 1.a reports the temperature program used, while Fig. 1.b and Fig. 1.c show the corrected values of the specific heat flow rate ($\dot{Q}$) and the enthalpy difference (ΔH). Catalysts clearly affect the development of the reactions modifying the peak distribution (Fig. 1.b) and the reaction enthalpy (Fig. 1.c); $FeCl_3$ and SRa show the greatest impact on the heat release. The addition of $FeCl_3$ makes the reaction start already after 15 min, corresponding to a temperature of 125 °C. The hydrolysis quickly develops reaching its maximum at a temperature of 145 °C with a heat flow rate of −0.6 mW/mg. This first peak runs out after 23.5 min from the start of the experiment when also the second peak starts. This second peak reaches its maximum heat flow rate of −2.5 mW/mg when the temperature hits 205 °C after 31 min. The reactions complete within the temperature ramp, which lasts 40 min. For all the other samples, reactions start only after 35 min. The addition of SRa leads to an overlapping of peak 1 and 2 showing a maximum heat flow rate of −1.1 mW/mg after 44 min. Since SRa is a mixture of alumina (60 %wt) and silica (40 %wt), a mixture of pure alumina and silica in the same proportion (AL60SI40) was prepared and tested to replicate SRa behavior, compare the catalytic effects and investigate the mechanism promoting synergies between acid and basic sites in the catalysts. As shown in Fig. 2, SRa and AL60SI40 impact the reaction in different ways, with SRa effect being more noticeable.

To better understand which of the sets of reactions are affected or promoted by the catalysts, a peak deconvolution was performed. In a previous study by the authors, three main curves were identified for cellulose, each corresponding to a set of reactions (Pecchi et al., 2022). Therefore, the same settings were used to perform the deconvolution, the results of which are shown in Fig. 3a-h. When comparing experimental and deconvoluted results (denoted as Exp. and Best fit, respectively), deconvoluted curves associated to RC, RM, SI showed slightly more inflections than the experimental ones. This is due to the baseline subtraction procedure, which causes a sharper onset on those curves preventing peak 2 from shifting slightly to the left as that would increase the error at the curve onset. However, since for all samples an R^2 between 97.2 and 99.7 was achieved, results were considered satisfactory.

Fig. 4 reports the time corresponding to the peak center and the

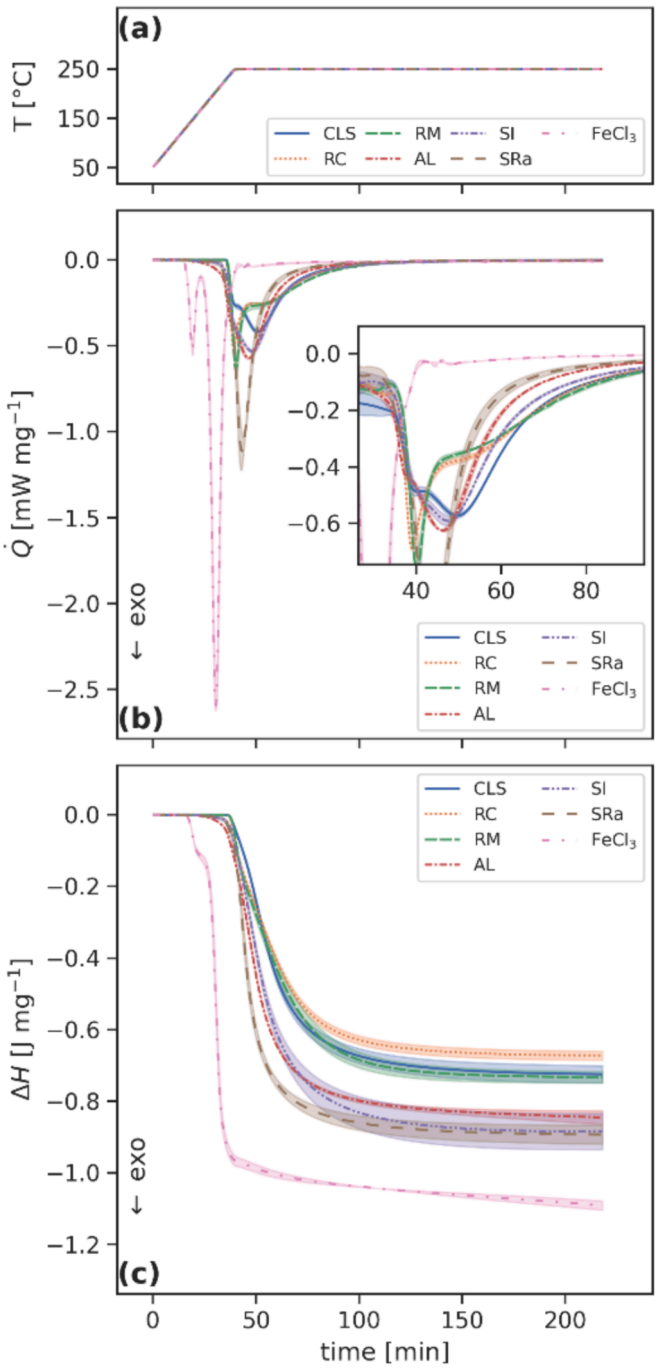

Fig. 1. DSC analysis of cellulose with and without catalysts. Fig. 1.a reports the temperature program, Fig. 1.b and Fig. 1.c the corrected values for the specific heat flow rate (Q) and reaction enthalpy (ΔH). The central lines represent the average values and the shaded areas the standard deviations (measurements were performed twice). Negative values are exothermic.

enthalpy of the deconvoluted $\dot{Q}$ peaks, obtained for the different runs with different catalysts. Error bars represent the standard deviation of deconvolution applied to different $\dot{Q}$ replicates.

Fig. 3a, shows the results obtained for pure cellulose where three curves can be identified corresponding to hydrolysis, hydroxymethylfurfural (HMF) polymerization and bulk carbonization, as previously stated.

Fig. 3b and c show how the addition of RC and RM promoted cellulose hydrolysis and bulk carbonization, while decreasing HMF polymerization. Looking at the results of pure cellulose, RC and RM in Fig. 4,

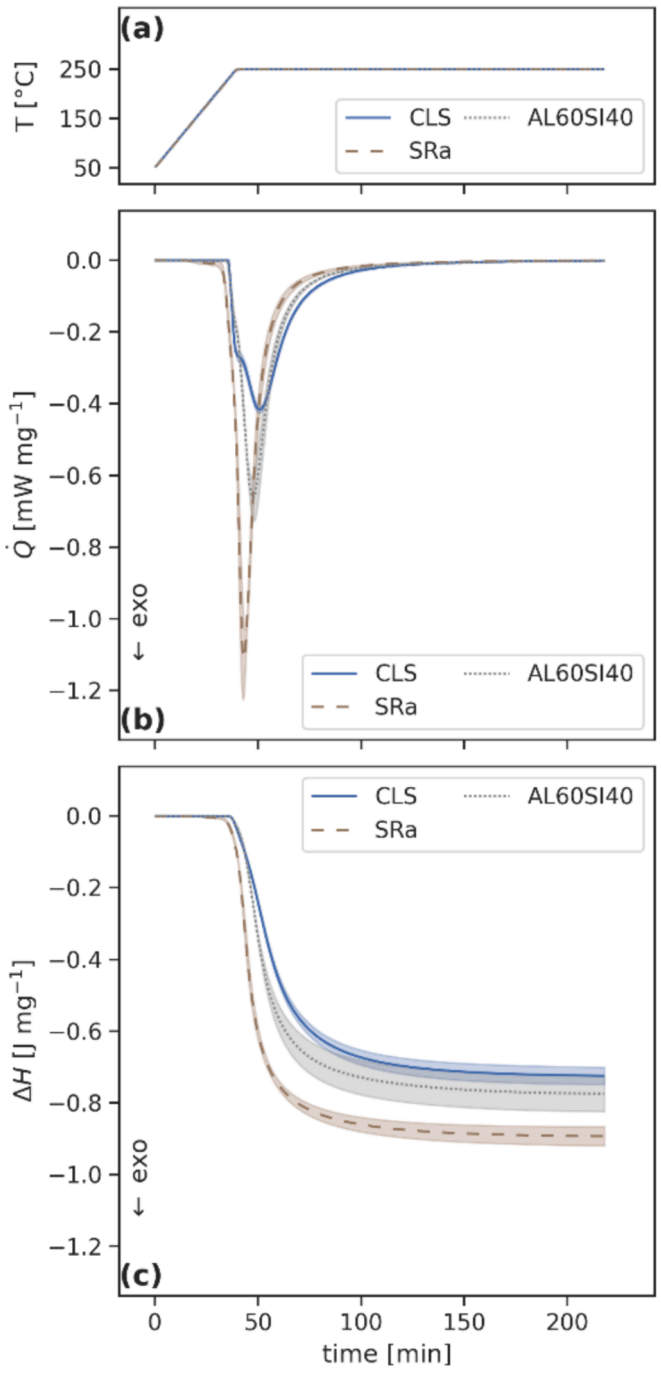

Fig. 2. DSC analysis results obtained when comparing the effects of Siralox and a mixture of silica (40 %wt) and alumina (60 %wt). The central lines represent the average values and the shaded areas the standard deviations (measurements were performed twice). Negative values are exothermic.

it is possible to note how the two catalysts only influence enthalpies, without substantially affecting timings. Indeed, enthalpies related to peaks 1 and 3 are higher for RC and RM than cellulose, while enthalpies related to peak 2 are lower. RC and RM are the only catalysts showing a decrease in the enthalpy of peak 2 and this might be related to the synergetic effects of their constituents that are similar. A similar correlation has been found by Cheng et al., whose work describes the activity of a catalysts as the result not only of physical properties such as surface area, and particle size, but also of the interaction among constituents, presence of dopants, and density and strength of both acid and base sites (Cheng et al., 2020). In the same work, it was found that RC and RM show base-acid site density ratios in the range of 50–150 corresponding to the highest values of biocrude oil energy recovery. Outside of this range, the energy recovery drops, as for the case of SiO_2 (base-acid site density ratio < 0.002) and Al_2O_3 (base-acid site density ratio equal to 260) (Cheng et al., 2020). As a consequence of the interactions between acid and basic sites, RC and RM hinder char formation affecting polymerization and carbonization (Cheng et al., 2020).

According to Fig. 3d and Fig. 4, AL addition tends to slightly suppress hydrolysis and promote depolymerization and carbonization anticipating the reactions and decreasing the corresponding enthalpies. SI (shown in Fig. 3e) seems to have the same effect as AL except for the timing of peak 3 more similar to the one of cellulose. However, when considering SRa (shown in Fig. 3f), a mixture of AL and SI, the effect on the reaction is more prominent. This might be due to the absence of synergies among acidic and basic sites in SI (mainly acidic) and AL (mainly basic), that are in fact present in the case of SRa. Indeed, in case of SRa addition, peak 1 is strongly reduced, but it is not anticipated, peak 2 is reduced, and it is anticipated, peak 3 is slightly reduced, but strongly anticipated (see Fig. 4). Moreover, it is worth noticing that the reaction time for pure cellulose is longer than 100 min, while it becomes almost 40 min shorter thanks to SRa addition. Therefore, providing information on the duration of the reaction, this methodology offers also the opportunity to optimize the overall process.

Considering mixtures of SI and AL (Fig. 3g), as already shown in Fig. 2, it was not possible to replicate SRa behavior even considering the same AL and SI proportions. In particular, as reported in Fig. 4, AL60SI40 addition decreased enthalpy of peak 1 and increased enthalpies of peak 2 and 3 like AL, SI and SRa, and anticipated peak 2 like AL and SRa, but to a different extent. This behavior can be related to the presence of both acidic and basic sites in AL60SI40 that are although different from the ones in SRa. For this reason, further characterization of the catalysts was conducted to clarify this issue and highlight the differences among the two materials.

Among all the catalysts tested, $FeCl_3$ (see Fig. 3h) showed the most remarkable effect: All reactions were anticipated, enthalpy of peak 1 and 3 increased and enthalpy of peak 2 decreased. The catalytic effect of $FeCl_3$ is bound to its constituents Fe3 + and Cl− (see Fig. 4). Fe3 + promotes the production of Lewis acid sites that would enhance decarboxylation and decarbonylation reactions and catalyze the glucose/fructose isomerization (Djandja et al., 2023), while Cl- could strongly interact with the end –OH group of monosaccharide units in cellulose enhancing the breaking of inter- and intramolecular hydrogen bonds and thus improving hydrolysis (Srilek et al., 2022). In agreement with Fig. 3.e, the isomerization of glucose/fructose is expected to take place at 110 °C with further formation of HMF via dehydratiation (Djandja et al., 2023). Also, the formation of acetic acid from HMF takes place between 110 – 120 °C and thus, these reactions were assigned to peak 1 (Djandja et al., 2023). The High Perfomance Liquid Cromatography (HPLC) results of the process water from HTC experiments of cellulose performed by Hammerton et al. confirm the above-mentioned hypothesis (Hammerton and Ross, 2022). They found that adding 0.1 M $FeCl_3$ makes the HPLC detect a large amount of glucose and HMF already at 100 °C (Hammerton and Ross, 2022). The formation of levulinic acid and formic acid is promoted by $FeCl_3$ too, and starts at 200 °C, which corresponds to the beginning of peak 2. These acids then condense and polymerize to form hydrochar (peak 3). These hypotheses are confirmed by Hammerton et al. (Hammerton and Ross, 2022). The HPLC results highlight that at 200 °C levulinic acid, formic acid, and acetic acid are formed (Hammerton and Ross, 2022). Furthermore, at 250 °C, formic acid disappears, confirming that it condenses to form hydrochar (Hammerton and Ross, 2022). Overall, the reaction appears to be over before the beginning of the isothermal step, meaning that it takes place during the heating ramp, while with pure cellulose the hydrolysis peak occurs at the end of the ramp and the reaction complete after more than 50 min.

The results confirm that it is possible to appreciate how different

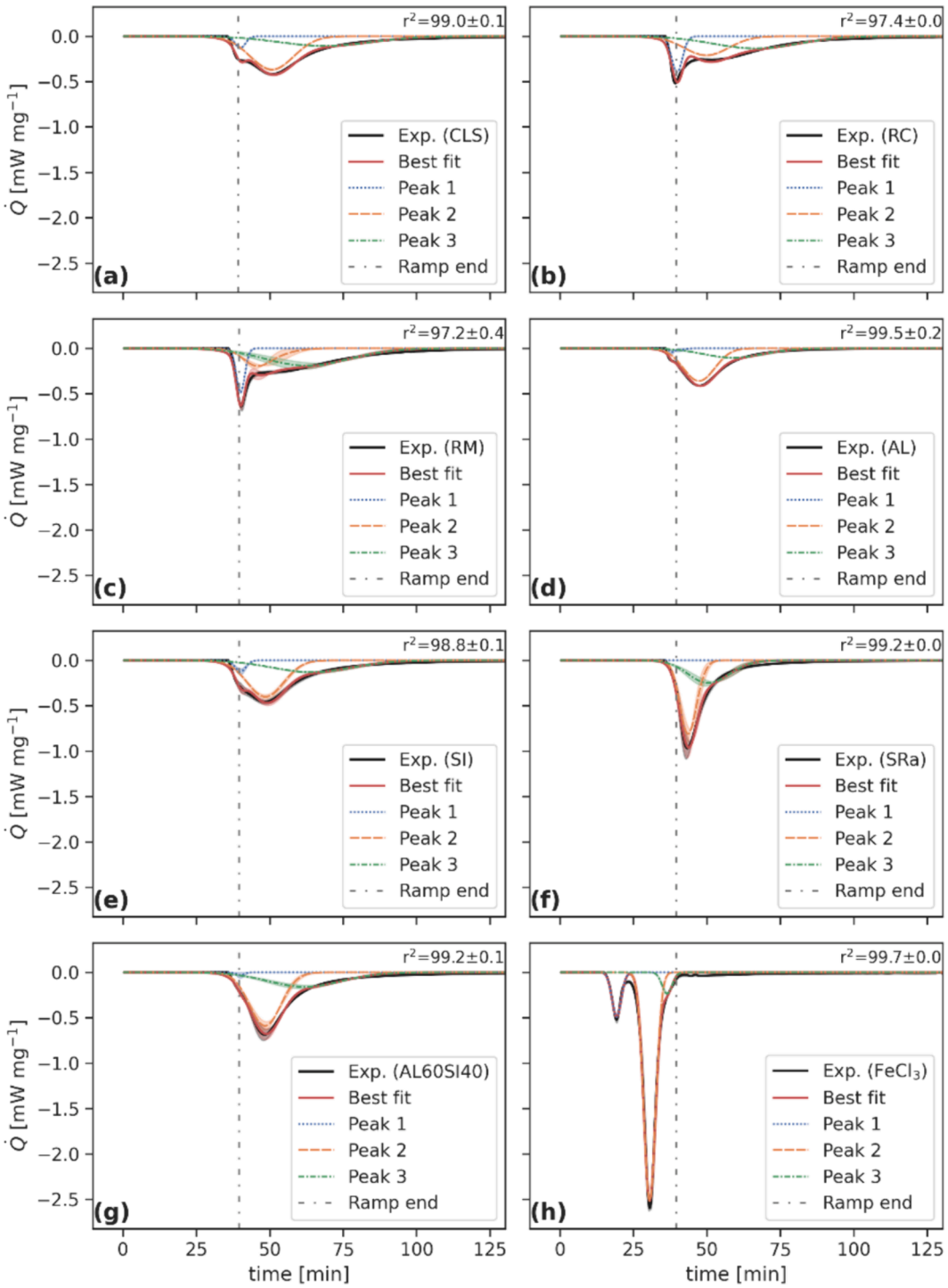

Fig. 3. Peak deconvolution applied to $\dot{Q}$ for the different runs with different catalysts. Exp.: experimental data obtained from the DSC of cellulose or cellulose with catalysts. Best fit: combination of deconvolution peaks. Peak 1, 2, 3: average results for deconvolution peaks with standard deviations (shaded areas) of the two replicates. Ramp end: end of the heating ramp of the DSC temperature program, located when 99% of the final temperature is reached.

catalysts affect the development of hydrothermal reactions using DSC. From a preliminary assessment of the results, it is possible to affirm that if the objective is to reduce the reaction time, $FeCl_3$ and SRa will be the most suitable candidates to be tested in scaled-up systems.

3.2. Synergies investigation

As discussed in section 3.1, when comparing the effect of SRa and AL60SI40, which is a mixture of SI and AL with the same proportions as in SRa, the results are far from being comparable. Hence, this section aims at investigating the differences in structure and composition that might promote or inhibit the synergies among the different components. XRD and FTIR-ATR results comparing SRa and AL60SI40 can be found in the Supplementary Material along with results obtained for other samples.

XRD results associated to AL60SI40 and SRa are similar, with AL60SI40 showing a more noticeable contribution of alumina in the range 30-40° (γ-alumina). Also, according to the FTIR-ATR analysis,

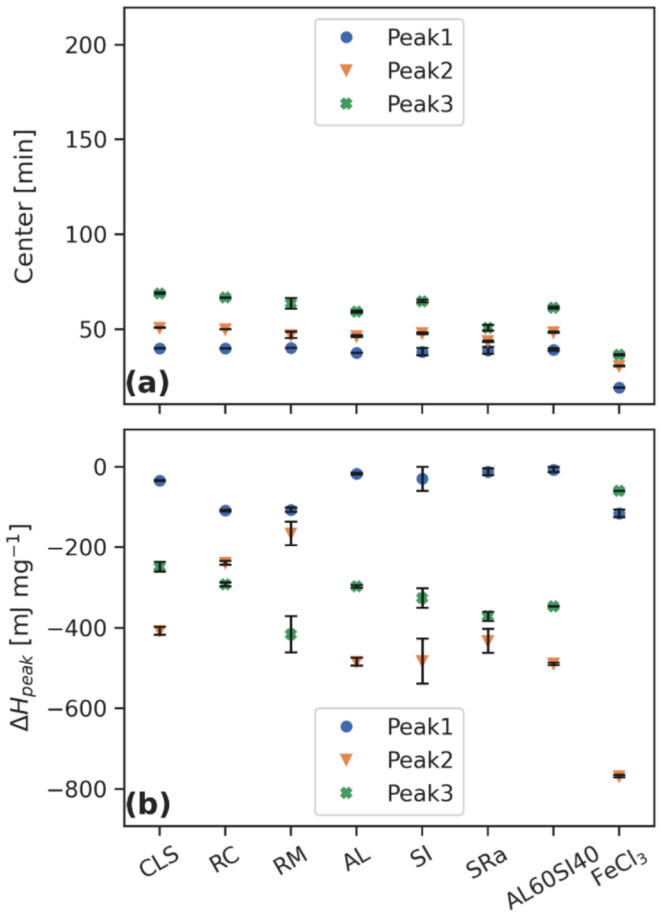

Fig. 4. Time corresponding to the peak center and enthalpy of deconvoluted peaks from $\dot{Q}$, obtained for the different runs with different catalysts. Error bars represent the standard deviation of the deconvolution applied to different $\dot{Q}$ duplicates.

there are no remarkable differences between SRa and the mixture, both showing overlapping peaks in the range 2000–500 cm^{-1}. The different behavior of the two samples in the DSC tests might be related to the different spatial distribution of the components (Cheng et al., 2020; Yu et al., 2011). As far as SRa is concerned, both silica and alumina are most likely always present in the same reaction site since they are mixed at the nanoscale. On the other hand, in the case of AL60SI40, silica and alumina are mixed only at the macro-scale. For this reason, the presence of both the components in the reaction site is not guaranteed and thus synergy is affected (Cheng et al., 2020). The hypothesis of a non-homogeneous distribution of silica and alumina within the reaction sites of AL60SI40, is also supported by the FTIR-ATR results showing a higher standard deviation for AL60SI40 than SRa, indicating that different proportions of AL and SI were evaluated during each repetition.

4. Conclusions

High pressure differential scanning calorimetry is used for the in-situ screening of catalysts for the conversion of biomass into biofuels using hydrothermal carbonization, based on their heat release profiles. The advantages are the short preparation time, the minor consumable cost, and the absence of chemical analysis; allowing to reduce the necessity for bench scale experiments and further characterization. The technique has been applied to heterogeneous catalysts, among which $FeCl_3$ showed the potential to significantly anticipate the reactions, while RC and RM confirmed how base-acid density ratio of the catalysts could influence the reaction pathways.

CRediT authorship contribution statement

Vittoria Benedetti: Writing – original draft, Validation, Methodology, Investigation, Formal analysis, Data curation, Conceptualization. **Alessandro Cascioli:** Writing – original draft, Visualization, Validation, Software, Methodology, Investigation, Formal analysis, Data curation, Conceptualization. **Matteo Pecchi:** Writing – review & editing, Software, Methodology, Conceptualization. **Marco Baratieri:** Writing – review & editing, Supervision, Resources, Project administration, Funding acquisition, Conceptualization.

Declaration of competing interest

The authors declare that they have no known competing financial interests or personal relationships that could have appeared to influence the work reported in this paper.

Data availability

Data will be made available on request.

Appendix A. Supplementary data

Supplementary data to this article can be found online at https://doi.org/10.1016/j.biortech.2024.130934.

References

Akbari, A., Peighambardoust, S.J., Lotfi, M., 2023. Hydrochar derived from Liquorice root pulp utilizing catalytic/non-catalytic hydrothermal carbonization: RSM optimization and cationic dye adsorption assessment. J. Water Process Eng. 55 https://doi.org/10.1016/j.jwpe.2023.104099.

Castello, D., Pedersen, T.H., Rosendahl, L.A., 2018. Continuous hydrothermal liquefaction of biomass: A critical review. Energies (basel). https://doi.org/10.3390/en11113165.

Chen, F., Zhang, Y., Zheng, M., Xiao, Y., Hu, H., Liang, Y., Liu, Y., Dong, H., 2022. Preparation of High-Performance Porous Carbon Materials by Citric Acid-Assisted Hydrothermal Carbonization of Bamboo and Their Application in Electrode Materials. Energy Fuel 36, 9303–9312. https://doi.org/10.1021/acs.energyfuels.2c01828.

Cheng, F., Tompsett, G.A., Murphy, C.M., Maag, A.R., Carabillo, N., Bailey, M., Hemingway, J.J., Romo, C.I., Paulsen, A.D., Yelvington, P.E., Timko, M.T., 2020. Synergistic Effects of Inexpensive Mixed Metal Oxides for Catalytic Hydrothermal Liquefaction of Food Wastes. ACS Sustain. Chem. Eng. 8, 6877–6886. https://doi.org/10.1021/acssuschemeng.0c02059.

Djandja, O.S., Liew, R.K., Liu, C., Liang, J., Yuan, H., He, W., Feng, Y., Lougou, B.G., Duan, P.G., Lu, X., Kang, S., 2023. Catalytic hydrothermal carbonization of wet organic solid waste: A review. Sci. Total Environ. https://doi.org/10.1016/j.scitotenv.2023.162119.

European Environment Agency, 2020. Bio-waste in Europe — turning challenges into opportunities.

Faradilla, R.F., Lucia, L., Hakovirta, M., 2020. Remarkable physical and thermal properties of hydrothermal carbonized nanoscale cellulose observed from citric acid catalysis and acetone rinsing. Nanomaterials 10. https://doi.org/10.3390/nano10061049.

Hammerton, J.M., Ross, A.B., 2022. Inorganic Salt Catalysed Hydrothermal Carbonisation (HTC) of Cellulose. Catalysts 12. https://doi.org/10.3390/catal12050492.

Ischia, G., Cazzanelli, M., Fiori, L., Orlandi, M., Miotello, A., 2022. Exothermicity of hydrothermal carbonization: Determination of heat profile and enthalpy of reaction via high-pressure differential scanning calorimetry. Fuel 310. https://doi.org/10.1016/j.fuel.2021.122312.

Kellicutt, A.B., Salary, R., Abdelrahman, O.A., Bond, J.Q., 2014. An examination of the intrinsic activity and stability of various solid acids during the catalytic decarboxylation of γ-valerolactone. Cat. Sci. Technol. 4, 2267–2279. https://doi.org/10.1039/c4cy00307a.

Kumar, M., Olajire Oyedun, A., Kumar, A., 2018. A review on the current status of various hydrothermal technologies on biomass feedstock. Renew. Sustain. Energy Rev. 81, 1742–1770. https://doi.org/10.1016/j.rser.2017.05.270.

Libra, J.A., Ro, K.S., Kammann, C., Funke, A., Berge, N.D., Neubauer, Y., Titirici, M.-M., Fühner, C., Bens, O., Kern, J., Emmerich, K.-H., 2011. Hydrothermal carbonization of biomass residuals: a comparative review of the chemistry, processes and applications of wet and dry pyrolysis. Biofuels 2, 71–106. https://doi.org/10.4155/bfs.10.81.

Liu, C., Kong, L., Wang, Y., Dai, L., 2018. Catalytic hydrothermal liquefaction of spirulina to bio-oil in the presence of formic acid over palladium-based catalysts. Algal Res. 33, 156–164. https://doi.org/10.1016/j.algal.2018.05.012.

Mahmood Al-Nuaimy, M.N., Azizi, N., Nural, Y., Yabalak, E., 2023. Recent advances in environmental and agricultural applications of hydrochars: A review. Environ. Res. 117923 https://doi.org/10.1016/j.envres.2023.117923.

Newville, M., Stensitzki, T., Allen, D.B., Ingargiola, A., 2014. LMFIT: Non-Linear Least-Square Minimization and Curve-Fitting for Python. 10.5281/zenodo.11813.

Pecchi, M., Patuzzi, F., Benedetti, V., Di Maggio, R., Baratieri, M., 2020a. Thermodynamics of hydrothermal carbonization: Assessment of the heat release profile and process enthalpy change. Fuel Process. Technol. 197, 106206 https://doi.org/10.1016/j.fuproc.2019.106206.

Pecchi, M., Patuzzi, F., Benedetti, V., Di, R., Baratieri, M., 2020b. Kinetic analysis of hydrothermal carbonization using high-pressure di ff erential scanning calorimetry applied to biomass. Appl. Energy 265, 114810. https://doi.org/10.1016/j.apenergy.2020.114810.

Pecchi, M., Cascioli, A., Maag, A.R., Goldfarb, J.L., Baratieri, M., 2022. Uncovering the Transition between Hydrothermal Carbonization and Liquefaction using differential scanning calorimetry. Fuel Process. Technol. 235, 107349 https://doi.org/10.1016/j.fuproc.2022.107349.

Ross, A.B., Biller, P., Kubacki, M.L., Li, H., Lea-Langton, A., Jones, J.M., 2010. Hydrothermal processing of microalgae using alkali and organic acids. Fuel 89, 2234–2243. https://doi.org/10.1016/j.fuel.2010.01.025.

Sharma, N., Jaiswal, K.K., Kumar, V., Vlaskin, M.S., Nanda, M., Rautela, I., Tomar, M.S., Ahmad, W., 2021. Effect of catalyst and temperature on the quality and productivity of HTL bio-oil from microalgae: A review. Renew. Energy. https://doi.org/10.1016/j.renene.2021.04.147.

Sharma, S.K., Parikh, P.A., Jasra, R.V., 2007. Solvent free aldol condensation of propanal to 2-methylpentenal using solid base catalysts. J. Mol. Catal. A Chem. 278, 135–144. https://doi.org/10.1016/j.molcata.2007.09.002.

Srilek, N., Aggarangsi, P., Pattiya, A., Tippayawong, N., 2022. Influence of chloride and propionate anions on properties of corn hydrochar from hydrothermal carbonization and activation. Biomass Convers. Biorefin. https://doi.org/10.1007/s13399-022-02460-x.

Sudibyo, H., Budhijanto, B., Marbelia, L., Güleç, F., Budiman, A., 2024. Kinetic and thermodynamic evidences of the Diels-Alder cycloaddition and Pechmann condensation as key mechanisms of hydrochar formation during hydrothermal conversion of Lignin-Cellulose. Chem. Eng. J. 480 https://doi.org/10.1016/j.cej.2023.148116.

Sushil, S., Batra, V.S., 2008. Catalytic applications of red mud, an aluminium industry waste: A review. Appl Catal B. https://doi.org/10.1016/j.apcatb.2007.12.002.

Timko, M.T., Ghoniem, A.F., Green, W.H., 2015. Upgrading and desulfurization of heavy oils by supercritical water. J. Supercrit. Fluids 96, 114–123. https://doi.org/10.1016/j.supflu.2014.09.015.

Weingarten, R., Tompsett, G.A., Conner, W.C., Huber, G.W., 2011. Design of solid acid catalysts for aqueous-phase dehydration of carbohydrates: The role of Lewis and Brønsted acid sites. J. Catal. 279, 174–182. https://doi.org/10.1016/j.jcat.2011.01.013.

World Energy Transitions Outlook 2022, 2022.

Yu, X., Yu, X., Wu, S., Liu, B., Liu, H., Guan, J., Kan, Q., 2011. The effect of the distance between acidic site and basic site immobilized on mesoporous solid on the activity in catalyzing aldol condensation. J. Solid State Chem. 184, 289–295. https://doi.org/10.1016/j.jssc.2010.11.007.

Yue, M., Lambert, H., Pahon, E., Roche, R., Jemei, S., Hissel, D., 2021. Hydrogen energy systems: A critical review of technologies, applications, trends and challenges. Renew. Sustain. Energy Rev. https://doi.org/10.1016/j.rser.2021.111180.

Zhang, C., Wang, X., Shao, M., Li, H., Chen, Q., Wang, N., Xu, Q., 2022. Synthesis of nitrogen-enriched hydrochar via co-hydrothermal reaction of liquid digestate and corn stalk. Sci. Total Environ. 836 https://doi.org/10.1016/j.scitotenv.2022.155572.

Zhang, B., Zhang, S.X., Yao, R., Wu, Y.H., Qiu, J.S., 2021. Progress and prospects of hydrogen production: Opportunities and challenges. J. Electron. Sci. Technol. 19, 1–15. https://doi.org/10.1016/J.JNLEST.2021.100080.